On the limit velocity and buckling phenomena of axially moving orthotropic membranes and plates

N. Banichuk[a], J. Jeronen[b], M. Kurki[b], P. Neittaanmäki[b], T. Saksa[b], T. Tuovinen[b,*]

[a] *Institute for Problems In Mechanics,Russian Academy of Sciences, Prospekt Vernadskogo 101, 119526 Moscow, Russia*

[b] *Department of Mathematical Information Technology, University of Jyväskylä, Mattilanniemi 2 (Agora), 40014 University of Jyväskylä, Finland*

Abstract

In this paper, we consider the static stability problems of axially moving orthotropic membranes and plates. The study is motivated by paper production processes, as paper has a fiber structure which can be described as orthotropic on the macroscopic level. The moving web is modelled as an axially moving orthotropic plate. The original dynamic plate problem is reduced to a two-dimensional spectral problem for static stability analysis, and solved using analytical techniques. As a result, the minimal eigenvalue and the corresponding buckling mode are found. It is observed that the buckling mode has a shape localized in the regions close to the free boundaries. The localisation effect is demonstrated with the help of numerical examples. It is seen that the in-plane shear modulus affects the strength of this phenomenon. The behaviour of the solution is investigated analytically. It is shown that the eigenvalues of the cross-sectional spectral problem are nonnegative. The analytical approach allows for a fast solver, which can then be used for applications such as statistical uncertainty and sensitivity analysis, real-time parameter space exploration, and finding optimal values for design parameters.

*Corresponding author

Email addresses: banichuk@ipmnet.ru (N. Banichuk), juha.jeronen@jyu.fi (J. Jeronen), matti.m.kurki@jyu.fi (M. Kurki), pn@mit.jyu.fi (P. Neittaanmäki), tytti.j.saksa@jyu.fi (T. Saksa), tero.t.tuovinen@jyu.fi (T. Tuovinen)

Keywords: Buckling, Axially Moving, Orthotropic, Shear modulus, Membrane, Plate

1. Introduction

As is well known, the mechanical behaviour of paper under a non-failure condition is adequately described by the model of an elastic orthotropic plate. The rigidity coefficients of the plate model, describing the tension and bending of the paper sheet, have been estimated for various types of paper in many publications (see, for example, Göttsching and Baumgarten, 1976; Thorpe, 1981; Skowronski and Robertson, 1985; Seo, 1999). The deformation properties of a sheet of paper under tensile stress or strain are used in simulation of axial movement of a paper web. In particular, these properties are important for modelling the instability of the axially moving elastic web.

There are numerous studies on the loss of stability of moving elastic webs based on one-dimensional models, using second- and fourth-order differential equations. These studies are devoted to various aspects of free and forced vibrations, including the nature of wave propagation in moving media, and the effects of axial motion on the frequency spectrum and eigenfunctions. The studies include e.g. Archibald and Emslie (1958), Miranker (1960), Swope and Ames (1963), Mote (1968), Mote (1972), Mote (1975), Simpson (1973), Ulsoy and Mote (1980), Ulsoy and Mote (1982), Chonan (1986), and Wickert and Mote (1990).

Two-dimensional studies have also been performed. Lin and Mote (1995) studied an axially moving membrane in a 2D formulation, predicting the equilibrium displacement and stress distributions under transverse loading. Later, the same authors predicted the wrinkling instability and the corresponding wrinkled shape of a web with small flexural stiffness (Lin and Mote, 1996). The stability and vibration characteristics of an axially moving plate were investigated by Lin (1997). The loss of stability was studied with application of

dynamic and static approaches and the approach by Wickert and Mote (1990) to derive the equation of motion for the plate in matrix form and to use the Galerkin method. It was shown by means of numerical analysis that, for all cases dynamic instability (flutter) is realised when the frequency is zero and the critical velocity coincides with the corresponding velocity obtained from static analysis. In Shin et al. (2005), the out-of-plane vibration of an axially moving membrane was studied. Also here, it was found by numerical analysis, that for a membrane with a no-friction boundary condition in the lateral direction along the rollers, the membrane remains dynamically stable until the critical speed, at which statical instability occurs.

The two-dimensional problem of instability analysis of an axially moving elastic plate was formulated and investigated analytically in Banichuk et al. (2010) in the context of the isotropic model. It was observed that the transverse deflection localizes near the free edges. This was noted to correspond to the eigenfunctions of stationary plates under in-plane compressive load (see, e.g., Gorman, 1982), and the results matched the above mentioned results of Lin (1997) and Shin et al. (2005) for moving plates and membranes.

Hatami et al. (2009) studied free vibration of the moving orthotropic rectangular plate in sub- and super-critical speeds, and flutter and divergence instabilities at supercritical speeds. Their study was limited to simply supported boundary conditions at all edges. Free vibrations of orthotropic rectangular plates, which are not moving, have been studied by Biancolini et al. (2005) including all combinations of simply supported and clamped boundary conditions on the edges. Xing and Liu (2009) obtained exact solutions for free vibrations of stationary rectangular orthotropic plates considering three combinations of simply supported (S) and clamped (C) boundary conditions: SSCC, SCCC and CCCC. Kshirsagar and Bhaskar (2008) studied vibrations and buckling of loaded stationary orthotropic plates. They found critical loads of buckling for all combinations of boundary conditions S, C and F.

In this paper, the analysis from Banichuk et al. (2010) is generalized to the case

of orthotropic material. Paper materials are an example of this, since they have a fiber structure which can be described as orthotropic on the macroscopic level. To understand the behaviour of such materials, it is thus important to consider in which ways and how much the introduction of the orthotropic material model changes the predictions with respect to those from the isotropic model. We develop an analytical solution for the orthotropic case, analogous to the isotropic development in our earlier study. Only a transcendental equation needs to be solved numerically. This allows for a fast solver, which can then be used for applications such as statistical uncertainty and sensitivity analysis, real-time parameter space exploration, and finding optimal values for design parameters.

The problem of stability of an axially moving orthotropic elastic plate travelling between two rollers at a constant velocity, and experiencing small transverse vibrations, is considered in a two-dimensional formulation. The model of a thin elastic orthotropic plate, which is subjected to bending and tension, is used for describing the bending moment and the distribution of membrane forces. The static form of instability is investigated and the critical regime is studied as a function of geometric parameters and the moduli of orthotropicity. It is shown that for some values of the problem parameters, the buckling mode becomes localized in the vicinity of the free boundaries also for the orthotropic plate.

It is well known that by using Huber's estimate for the shear modulus of an orthotropic plate, the equations reduce to those of the isotropic case. In this paper, it is briefly noted that this approach works also for the time-dependent dynamic equation of the moving plate. However, in the analysis proper, we will not make this assumption, but instead develop the analysis for the general orthotropic case.

Huber's estimate is not the only way to theoretically estimate the shear modulus. Methods such as calculating the Young modulus in the 45^{o} direction based on laminate theory, and Campbell's estimate have been used (Yokoyama and

Nakai, 2007). Thus, if we allow for the use of actual measured values for the shear modulus, it is possible to compare the different estimates. Also, this makes possible the sensitivity analysis of the shear modulus with respect to any deviation from the Huber estimate.

It should be noted that when applied to the particular context of paper production, this study still ignores some potentially important effects. First, damping effects resulting from the viscoelastic nature of paper are neglected. This is not a major problem, as the introduction of damping is not expected to change the critical velocity, although it does modify the postdivergence behaviour (Ulsoy and Mote, 1982). Secondly, the interaction between the travelling web and the surrounding air is known to influence the critical velocity (Pramila, 1986; Frondelius et al., 2006) and the dynamical response (Kulachenko et al., 2007), possibly also affecting the buckling shape. These effects are ignored by the in-vacuum model used in the present study.

2. Basic relations for transverse vibrations of an axially moving orthotropic band

Consider an elastic band travelling with a constant velocity V_0 in the x direction between two rollers located at $x = 0$ and $x = \ell$ in a Cartesian coordinate system. Figure 1 shows a rectangular part of the band

$$\Omega : \; 0 \leq x \leq \ell \,, \qquad -b \leq y \leq b \,,$$

where ℓ and b are prescribed parameters. Assume that the considered part of the band has constant thickness h.

Additionally assume that the band is represented as a rectangular elastic orthotropic plate having bending rigidities D_1, D_2 and D_3, or as a rectangular orthotropic membrane with zero bending rigidities. The "1" axis of the orthotropic material is aligned with the x direction, while the "2" axis is aligned with the y direction (see Figure 1). The band is subjected to homogeneous tension, acting in the x direction. The sides of the band $x = 0$, $-b \leq y \leq b$ and

$x = \ell$, $-b \leq y \leq b$ are simply supported, and the sides $y = -b$, $0 \leq x \leq \ell$ and $y = b$, $0 \leq x \leq \ell$ are free of tractions.

The transverse displacement of the travelling band is described by the deflection function w, which depends on the coordinates x, y and time t. The differential equation for small transverse vibrations has the form

$$m\left(\frac{\partial^2 w}{\partial t^2} + 2V_0\frac{\partial^2 w}{\partial x \partial t} + V_0^2\frac{\partial^2 w}{\partial x^2}\right) = T_{xx}\frac{\partial^2 w}{\partial x^2} + 2T_{xy}\frac{\partial^2 w}{\partial x \partial y} + T_{yy}\frac{\partial^2 w}{\partial y^2} - \mathcal{L}(w) \quad (1)$$

where

$$\mathcal{L}(w) = D_1\frac{\partial^4 w}{\partial x^4} + 2D_3\frac{\partial^4 w}{\partial x^2 \partial y^2} + D_2\frac{\partial^4 w}{\partial y^4}\,, \quad (2)$$

in the case of a plate. For the bending rigidities in (2), we have the expressions (see, e.g., Timoshenko and Woinowsky-Krieger, 1959, p. 365)

$$D_1 = \frac{h^3}{12}C_{11}\,, \quad D_2 = \frac{h^3}{12}C_{22}\,, \quad D_3 = \frac{h^3}{12}\left(C_{12} + 2\,C_{66}\right)\,, \quad (3)$$

where C_{ij} are the elastic moduli. These can be expressed in terms of the Young moduli E_1, E_2 and Poisson ratios ν_{12}, ν_{21} as (see, e.g., Kikuchi, 1986, p. 187–189)

$$C_{11} = \frac{E_1}{1-\nu_{12}\nu_{21}}\,,\; C_{22} = \frac{E_2}{1-\nu_{12}\nu_{21}}\,,\; C_{12} = C_{21} = \frac{\nu_{12}E_2}{1-\nu_{12}\nu_{21}}\,,\; C_{66} = G_{12}\,. \quad (4)$$

In (4), E_1 (respectively E_2) is the Young modulus in the x (respectively y) direction, ν_{12} (ν_{21}) is the Poisson ratio in the xy plane when the stretching is applied in the x (y) direction, and G_{12} is the shear modulus in the xy plane.

In the case of a membrane, the operator $\mathcal{L}$ in equation (1) is omitted ($\mathcal{L}(w) \equiv 0$). In equation (1), m is the mass per unit area of the middle surface of the band, and T_{xx}, T_{xy} and T_{yy} are the in-plane tensions.

We assume that the deflection function w and its partial derivatives are small, and that they satisfy the boundary conditions corresponding to simply supported boundaries at $x = 0$, $-b \leq y \leq b$ and $x = \ell$, $-b \leq y \leq b$, and free boundaries at $-b \leq y \leq b$, $0 \leq x \leq \ell$. In the case of an orthotropic plate, the boundary conditions read

$$(w)_{x=0,\ell} = 0, \qquad \left(\frac{\partial^2 w}{\partial x^2}\right)_{x=0,\ell} = 0\,, \qquad -b \leq y \leq b\,, \quad (5)$$

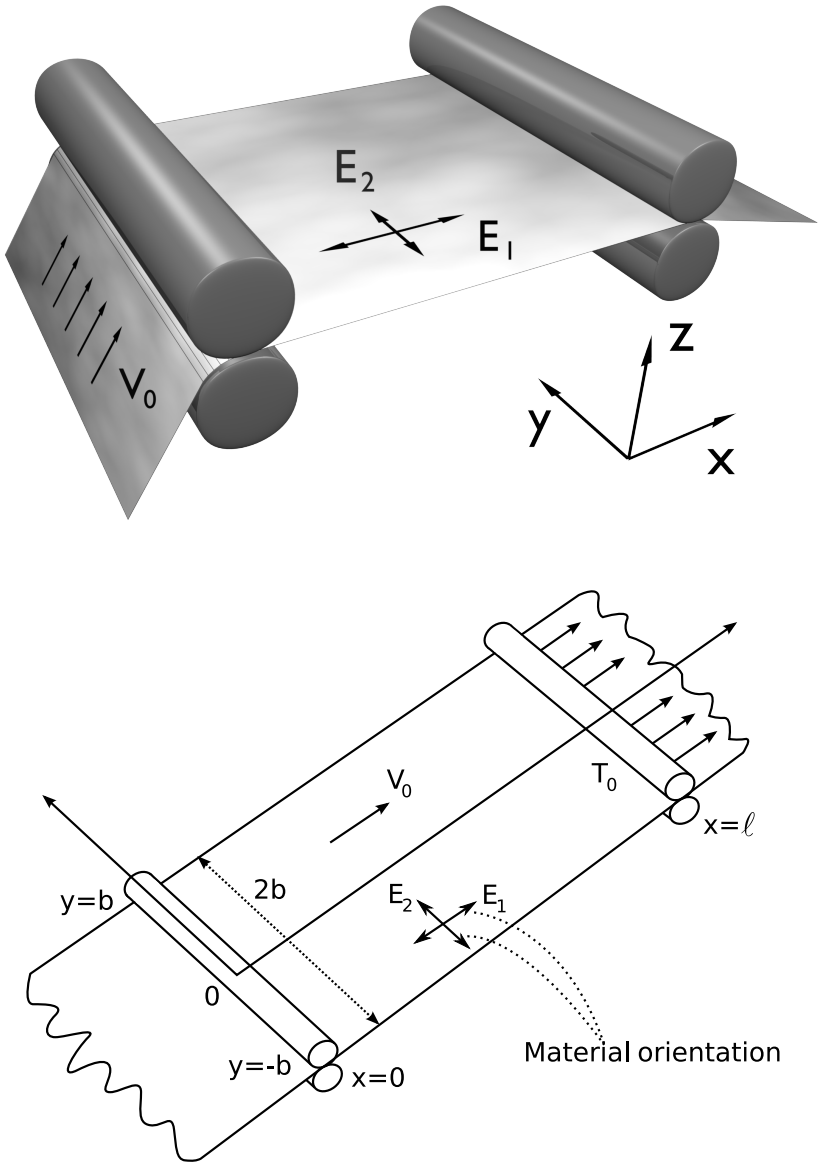

Figure 1: Axially moving elastic orthotropic band, simply supported at $x = 0$ and $x = \ell$.

$$\left(\frac{\partial^2 w}{\partial y^2} + \beta_1 \frac{\partial^2 w}{\partial x^2}\right)_{y=\pm b} = 0\,, \qquad 0 \le x \le \ell\,, \tag{6}$$

$$\left(\frac{\partial^3 w}{\partial y^3} + \beta_2 \frac{\partial^3 w}{\partial x^2 \partial y}\right)_{y=\pm b} = 0, \qquad 0 \le x \le \ell\,, \tag{7}$$

where β_1 and β_2 are mechanical parameters defined as

$$\beta_1 = \nu_{12}\,, \qquad \beta_2 = \nu_{12} + \frac{4\,G_{12}}{E_2}(1 - \nu_{12}\nu_{21})\,. \tag{8}$$

As is well known, in the isotropic case we have $E_1 = E_2 = E$, $\nu_{12} = \nu_{21} = \nu$, $G_{12} = G = E/(2(1+\nu))$ and, consequently, $\beta_1 = \nu$ and $\beta_2 = 2 - \nu$.

Huber (1923) showed that if the in-plane shear modulus G_{12} of an orthotropic plate is approximated by the geometric average

$$G_H \equiv \frac{\sqrt{E_1 E_2}}{2(1 + \sqrt{\nu_{12}\nu_{21}})}\,, \tag{9}$$

the equations reduce to those of the isotropic plate. It is easy to show that this property holds for the time-dependent plate problem including axial motion, too. Because coordinate scaling is only required in the y direction (see Timoshenko and Woinowsky-Krieger, 1959, p. 366 for the transformations), the Coriolis term w_{xt} generated by the axial motion of the plate introduces no trouble for this approach. For the rest of this article, unless otherwise noted, it is assumed that G_{12} is an independent material parameter.

In the case of a membrane, the boundary condition at the rollers reads

$$(w)_{x=0,\,\ell} = 0\,, \quad -b \le y \le b\,. \tag{10}$$

On the free edges, classical membrane theory asserts (see, e.g., Sagan, 1961; Weinstock, 2008 (reprint) $\left(\frac{\partial w}{\partial y}\right)_{y=\pm b} = 0$ $(0 \le x \le \ell)$. On the other hand, Shin et al. (2005) have used a different condition for zero traction, which does not contain the transverse displacement w. Below, we will see that in our case for a membrane, the choice of the boundary condition on the free edges does not matter.

For both the plate and membrane cases, in equation (1), T_{xx}, T_{xy} and T_{yy} are in-plane tensions related to the corresponding stress tensor components σ_{xx}, σ_{xy} and σ_{yy} by the expressions

$$T_{xx} = h\,\sigma_{xx}, \quad T_{xy} = h\,\sigma_{xy}, \quad T_{yy} = h\,\sigma_{yy}\,. \tag{11}$$

The in-plane stresses σ_{xx}, σ_{xy} and σ_{yy} are assumed to satisfy the standard equilibrium equations

$$\frac{\partial \sigma_{xx}}{\partial x} + \frac{\partial \sigma_{xy}}{\partial y} = 0, \quad \frac{\partial \sigma_{xy}}{\partial x} + \frac{\partial \sigma_{yy}}{\partial y} = 0\,. \tag{12}$$

with the boundary conditions

$$(\sigma_{xx})_{x=0,\,\ell} = T_0\,, \qquad \big(\sigma_{xy}\big)_{x=0,\,\ell} = 0\,, \qquad -b \le y \le b\,, \tag{13}$$

$$\big(\sigma_{yy}\big)_{y=\pm b} = 0\,, \qquad \big(\sigma_{xy}\big)_{y=\pm b} = 0\,, \qquad 0 \le x \le \ell\,, \tag{14}$$

where T_0 is prescribed positive parameter. Taking into account the behavioural equation of the plane theory of elasticity and the boundary conditions (13) and (14), we have for the considered orthotropic band the tension field

$$T_{xx} = T_0\,, \qquad T_{yy} = T_{xy} = 0\,, \qquad (x, y) \in \Omega\,. \tag{15}$$

As is well known, the in-plane displacements u, v, oriented respectively along the axes x and y, are related to the stresses by means of the generalized Hooke's Law

$$\sigma_{xx} = C_{11}\frac{\partial u}{\partial x} + C_{12}\frac{\partial v}{\partial y}\,,\ \sigma_{xy} = C_{66}\left(\frac{\partial u}{\partial y} + \frac{\partial v}{\partial x}\right)\,,\ \sigma_{yy} = C_{12}\frac{\partial u}{\partial x} + C_{22}\frac{\partial v}{\partial y}\,, \tag{16}$$

where C_{ij} are the elastic moduli (4). In the following, we will use Maxwell's relation

$$E_1\nu_{21} = E_2\nu_{12}\,. \tag{17}$$

In the computations, we will use E_1, E_2 and ν_{12} as independent parameters, and calculate ν_{21} from equation (17).

In this study, we will use a prescribed tension T_0. However, note that by using equations (12) and (16), it is possible to show that, if instead of a prescribed tension T_0 we have a prescribed displacement u_0 at $x = \ell$, the generated tension

field has the form (15) and its value is

$$T_0 = h\frac{u_0}{\ell}\left(C_{11} - \frac{C_{12}^2}{C_{22}}\right) = h\frac{u_0}{\ell}E_1\ . \tag{18}$$

Therefore, our results are applicable to this case, too.

The boundary conditions used in deriving (18) were (14) and the following: $\sigma_{xy} = 0$ at $x = 0, \ell$ and $u|_{x=0} = 0,\ u|_{x=\ell} = u_0$. By (4) and (17), the last form in (18) follows easily. We see that the only material parameter that affects the homogeneous tension field generated by the prescribed displacement is the Young modulus in the longitudinal direction. Compare (18) with $T_0 = h\frac{u_0}{\ell}E$ for an isotropic material.

For the computations, we introduce the characteristic bending rigidity D_0 (some positive constant) and the dimensionless bending rigidities

$$H_1 = \frac{D_1}{D_0}, \qquad H_2 = \frac{D_2}{D_0}, \qquad H_3 = \frac{D_3}{D_0}\ . \tag{19}$$

We will use the choice $D_0 = D_1$ below.

Equation (1) becomes

$$\frac{\partial^2 w}{\partial t^2} + 2V_0\frac{\partial^2 w}{\partial x \partial t} + \left(V_0^2 - C^2\right)\frac{\partial^2 w}{\partial x^2} + \frac{D_0}{m}\mathcal{L}_0(w) = 0, \qquad C = \sqrt{\frac{T_0}{m}}\ , \tag{20}$$

where

$$\mathcal{L}_0(w) = H_1\frac{\partial^4 w}{\partial x^4} + 2H_3\frac{\partial^4 w}{\partial x^2 \partial y^2} + H_2\frac{\partial^4 w}{\partial y^4}\ . \tag{21}$$

Note that the considered plate boundary value problem (20) – (21), (5) – (7), is homogeneous and invariant with respect to the symmetry operation $y \to -y$ and, consequently, all solutions of the problem can be considered as symmetric or antisymmetric functions of y, i.e.

$$w(x, y, t) = w(x, -y, t) \qquad \text{or} \qquad w(x, y, t) = -w(x, -y, t)\,. \tag{22}$$

3. Divergence velocity of a membrane

Consider the case of a rectangular orthotropic membrane. We omit the bending terms from (20):

$$\frac{\partial^2 w}{\partial t^2} + 2V_0 \frac{\partial^2 w}{\partial x \partial t} + \left(V_0^2 - C^2\right) \frac{\partial^2 w}{\partial x^2} = 0, \quad C = \sqrt{\frac{T_0}{m}} \,. \tag{23}$$

This equation is considered with the homogeneous boundary condition (10). Let us represent the solution of the dynamic boundary-value problem (23), (10), as (Bolotin, 1963)

$$w(x, y, t) = W(x, y) e^{i\omega t} \,, \tag{24}$$

or in the equivalent form

$$w(x, y, t) = W(x, y) e^{st} \,, \tag{25}$$

where ω is the frequency of small transverse vibrations and

$$s = i\,\omega \tag{26}$$

is the complex characteristic parameter. To investigate the dynamic behaviour of the membrane, we insert the representation (25) into equation (23) and boundary condition (10). We have

$$s^2 W + 2sV_0 \frac{\partial W}{\partial x} + \left(V_0^2 - C^2\right) \frac{\partial^2 W}{\partial x^2} = 0 \,, \tag{27}$$

$$(W)_{x=0,\,\ell} = 0 \,, \quad -b \le y \le b \,. \tag{28}$$

We multiply the left-hand side of equation (27) by W and perform integration over the domain Ω $(0 \le x \le \ell,\ -b \le y \le b)$ to obtain

$$s^2 \int_\Omega W^2 \, \mathrm{d}\Omega + 2sV_0 \int_\Omega W \frac{\partial W}{\partial x} \, \mathrm{d}\Omega + \left(V_0^2 - C^2\right) \int_\Omega W \frac{\partial^2 W}{\partial x^2} \, \mathrm{d}\Omega = 0 \,. \tag{29}$$

The second and third integrals in equation (29) are evaluated with the help of integration by parts and the boundary conditions (28). We have

$$\int_\Omega W \frac{\partial W}{\partial x} \, \mathrm{d}\Omega = 0 \,, \tag{30}$$

$$\int_\Omega W\frac{\partial^2 W}{\partial x^2}\,\mathrm{d}\Omega = -\int_\Omega \left(\frac{\partial W}{\partial x}\right)^2\,\mathrm{d}\Omega\,. \tag{31}$$

Using the equalities (29) – (31) and performing elementary transformations, we obtain the following expression for the characteristic index:

$$s^2 = \left(V_0^2 - C^2\right)\frac{\int_\Omega \left(\frac{\partial W}{\partial x}\right)^2\,\mathrm{d}\Omega}{\int_\Omega W^2\,\mathrm{d}\Omega}\,. \tag{32}$$

If s becomes zero, we have the steady state solution (buckling) with frequency $\omega = 0$ at some velocity $V_0 = V_0^{\mathrm{div}}$. The value of this divergence velocity is estimated as

$$V_0^{\mathrm{div}} = C = \sqrt{\frac{T_0}{m}} = \sqrt{\frac{hu_0}{m\ell}E_1}\,, \tag{33}$$

where in the last form equation (18) has been used.

4. Static analysis of stability loss of a plate

In the following, we will perform static analysis of stability loss of a plate. The problem is formulated as the eigenvalue problem for the partial differential equation

$$\left(mV_0^2 - T_0\right)\frac{\partial^2 w}{\partial x^2} + D_0\mathcal{L}_0(w) = 0 \tag{34}$$

with the boundary conditions (5) – (7). To determine the minimal eigenvalue,

$$\lambda = \gamma^2 = \frac{\ell^2}{\pi^2 D_0}\left(mV_0^2 - T_0\right)\,, \tag{35}$$

of the problem (5) – (7), (34), and the corresponding eigenfunction $w = w(x, y)$, known as the divergence or buckling form, we apply the following representation:

$$w = w(x, y) = f(y)\ \sin\left(\frac{\pi x}{\ell}\right)\,, \tag{36}$$

where $f\,(y)$ is an unknown function. The fact that the solution is a half-sine in the longitudinal direction is well-known in the isotropic case; see e.g. Lin (1997). It is easy to see that the same form is applicable for the orthotropic plate. What remains to be determined is the unknown cross-section $f(y)$.

It follows from (36) that the desired buckling form w satisfies the boundary conditions (5). Using dimensionless variables $\eta = \frac{y}{b}$ and $\mu = \frac{\ell}{\pi b}$ and the relations (6), (7), (34)-(36), we obtain the following eigenvalue problem for the unknown function $f(\eta)$:

$$\mu^4 H_2 \frac{\mathrm{d}^4 f}{\mathrm{d}\eta^4} - 2\mu^2 H_3 \frac{\mathrm{d}^2 f}{\mathrm{d}\eta^2} + (H_1 - \lambda) f = 0\,, \qquad -1 \le \eta \le 1\,, \tag{37}$$

$$\left(\mu^2 \frac{\mathrm{d}^2 f}{\mathrm{d}\eta^2} - \beta_1 f \right)_{\eta=\pm 1} = 0\,, \tag{38}$$

$$\left(\mu^2 \frac{\mathrm{d}^3 f}{\mathrm{d}\eta^3} - \beta_2 \frac{\mathrm{d} f}{\mathrm{d}\eta} \right)_{\eta=\pm 1} = 0\,. \tag{39}$$

We denote

$$\mathcal{L}_1(f) = \mu^4 H_2 \frac{\mathrm{d}^4 f}{\mathrm{d}\eta^4} - 2\,\mu^2 H_3 \frac{\mathrm{d}^2 f}{\mathrm{d}\eta^2} + H_1 f\,.$$

To show that the eigenvalues λ of $\mathcal{L}_1(f)$ are non-negative, we proceed using general ideas from Chen et al. (1998), who proved a similar result for an isotropic stationary plate.

We introduce the bilinear form $a(f, g)$ that corresponds to the strain energy of a plate (see Timoshenko and Woinowsky-Krieger, 1959, p. 377),

$$\begin{aligned} a(f,g) = \int_{-1}^{1} \Bigg[& H_1 f\, \bar{g} - \mu^2 B_1 f\, \frac{\mathrm{d}^2 \bar{g}}{\mathrm{d}\eta^2} - \mu^2 B_1 \frac{\mathrm{d}^2 f}{\mathrm{d}\eta^2}\, \bar{g} \\ & + \mu^4 H_2 \frac{\mathrm{d}^2 f}{\mathrm{d}\eta^2} \frac{\mathrm{d}^2 \bar{g}}{\mathrm{d}\eta^2} + 4\mu^2 B_2 \frac{\mathrm{d} f}{\mathrm{d}\eta} \frac{\mathrm{d}\bar{g}}{\mathrm{d}\eta} \Bigg] \mathrm{d}\eta\,, \end{aligned} \tag{40}$$

where

$$B_1 + 2\,B_2 = H_3\,.$$

Performing integration by parts on (40), we obtain

$$a(f,g) = \int_{-1}^{1} \left[\mu^4 H_2 \frac{\mathrm{d}^4 f}{\mathrm{d}\eta^4} - 2\,\mu^2 H_3 \frac{\mathrm{d}^2 f}{\mathrm{d}\eta^2} + H_1 f \right] \bar{g}\, \mathrm{d}\eta\,.$$

Thus, the form $a(f, g)$ can alternatively be defined as

$$a(f,g) \;=\; (\mathcal{L}_1(f), g)$$

where the inner product $(\cdot\,,\cdot\,)$ is

$$(u,v) \;=\; \int_{-1}^{1} u\,\bar{v}\,\mathrm{d}\eta\,.$$

The operator $\mathcal{L}_1(f)$ is easily seen to be self-adjoint, and the form $a(f,g)$ induces a positive semidefinite norm $a(f,f)$,

$$\begin{aligned} a(f,f) = \int_{-1}^{1} \Bigg[H_1 \left\| f - \mu^2 \nu_{21} \frac{\mathrm{d}^2 f}{\mathrm{d}\eta^2} \right\|^2 + \mu^4 H_2 (1 - \nu_{12}\nu_{21}) \left\| \frac{\mathrm{d}^2 f}{\mathrm{d}\eta^2} \right\|^2 \\ + 4\,\mu^2 B_2 \left\| \frac{\mathrm{d} f}{\mathrm{d}\eta} \right\|^2 \Bigg] \mathrm{d}\eta \;\geq 0\,. \end{aligned}$$

This implies that the eigenvalues of $\mathcal{L}_1(f)$ are nonnegative. That is,

$$\lambda \geq 0\,, \tag{41}$$

for all eigenvalues λ of the problem (37) – (39), which governs the cross-sectional eigenfunctions $f(y)$ and the corresponding eigenvalues of the buckled, moving orthotropic plate.

The particular solutions of the ordinary differential equation (37) have the form

$$f = A e^{p\eta}, \qquad p = \frac{\kappa}{\mu} \tag{42}$$

where A is an arbitrary constant and κ is a solution of the following biquadratic algebraic characteristic equation:

$$H_2\kappa^4 - 2H_3\kappa^2 + (H_1 - \lambda) = 0 \tag{43}$$

that is written as

$$\kappa_\pm^2 = \frac{H_3}{H_2}\left(1 \pm \sqrt{1 - \frac{H_2(H_1-\lambda)}{H_3^2}}\right) = \frac{H_3}{H_2}\left(1 \pm \sqrt{1 - \frac{H_2(1-\lambda)}{H_3^2}}\right)\,, \tag{44}$$

where the upper (lower) signs correspond to each other.

The solutions $\kappa_\pm$ are real-valued, if we have the following range for λ:

$$\lambda_{\min} \equiv 1 - \frac{H_3^2}{H_2} \leq \lambda \leq 1 \equiv \lambda_{\max}\,, \tag{45}$$

corresponding to a real-valued eigenfunction f. The lower limit $\lambda_{\min}$ is non-positive,

$$\lambda_{\min} \leq 0\,,$$

if

$$G_{12} \geq G_H\,.$$

By (41) and (45), in the case that the shear modulus G_{12} is greater than or equal to the geometric average shear modulus G_H, we may seek the lowest eigenvalue in the range

$$0 \leq \lambda \leq 1\,, \tag{46}$$

as was done in the isotropic case (Banichuk et al., 2010). On the other hand, it is also possible that

$$G_{12} < G_H$$

(for some measurements of G_{12} for paper materials, see Yokoyama and Nakai, 2007; Bonnin et al., 2000; Seo, 1999; Mann et al., 1980). In this case, we have

$$\lambda_{\min} \geq 0\,,$$

which will produce complex solutions $\kappa_\pm$ and complex eigenfunctions if λ is in the range

$$0 \leq \lambda \leq \lambda_{\min}\,.$$

Numerically, however, it is seen that this interval contains no solutions.

From (42), (44) we obtain that the general solution can be represented in the form

$$f(\eta) = A_1 e^{+\frac{\kappa_+}{\mu}\eta} + A_2 e^{-\frac{\kappa_+}{\mu}\eta} + A_3 e^{+\frac{\kappa_-}{\mu}\eta} + A_4 e^{-\frac{\kappa_-}{\mu}\eta} \tag{47}$$

with unknown constants A_1, A_2, A_3 and A_4.

The eigenvalue boundary value problem (37) – (39) is invariant under the symmetry operation $\eta \to -\eta$, and consequently the eigenforms (EFs) can be classified into functions that are symmetric, f^s, or antisymmetric, f^a, about the origin.

Using the relations (37) – (39), (47), we obtain a general representation for the function $f^s(\eta)$ and linear algebraic equations for determining the constants A^s and B^s:

$$f^s(\eta) = A^s \cosh\frac{\kappa_+\eta}{\mu} + B^s \cosh\frac{\kappa_-\eta}{\mu} \tag{48}$$

$$A^s\left(\kappa_+^2 - \beta_1\right)\cosh\frac{\kappa_+}{\mu} + B^s\left(\kappa_-^2 - \beta_1\right)\cosh\frac{\kappa_-}{\mu} = 0 \tag{49}$$

$$A^s\kappa_+\left(\kappa_+^2 - \beta_2\right)\sinh\frac{\kappa_+}{\mu} + B^s\kappa_-\left(\kappa_-^2 - \beta_2\right)\sinh\frac{\kappa_-}{\mu} = 0\,, \tag{50}$$

where A^s and B^s are unknown constants. Note that due to the symmetry (or antisymmetry) of the solution f, we have only two independent unknown constants, instead of the four in the general representation (47) where the symmetry considerations had not yet been applied.

The conditions for a non-trivial solution to exist in the form of (48) and (49), (50) reduce to the determinant of the homogeneous system (49), (50) vanishing. The zero determinant condition can be expressed as

$$\Phi(\gamma, \mu, \nu_{12}, E_1, E_2, G_{12}) - \Psi(\gamma, \nu_{12}, E_1, E_2, G_{12}) = 0\,, \tag{51}$$

where

$$\Phi(\gamma, \mu, \nu_{12}, E_1, E_2, G_{12}) = \tanh\frac{\kappa-}{\mu}\coth\frac{\kappa_+}{\mu}\,, \tag{52}$$

$$\Psi(\gamma, \nu_{12}, E_1, E_2, G_{12}) = \frac{\kappa_+(\kappa_+^2 - \beta_2)(\kappa_-^2 - \beta_1)}{\kappa_-(\kappa_+^2 - \beta_1)(\kappa_-^2 - \beta_2)}\,. \tag{53}$$

$$\kappa_+ = \kappa_+(\gamma, \nu_{12}, E_1, E_2, G_{12}), \qquad \kappa_- = \kappa_-(\gamma, \nu_{12}, E_1, E_2, G_{12})\,.$$

This equation can be used to determine the eigenvalues $\lambda = \gamma^2$ corresponding to symmetric eigenfunctions with different values of the parameters μ, ν_{12}, E_1, E_2 and G_{12}. Note that there is no dependence on the parameter ν_{21}, since it depends on ν_{12}, E_1 and E_2 via Maxwell's relation (17).

Similarly, using the relations (38) and (39), we can obtain a representation for antisymmetric eigenfunctions $f^a(\eta)$, the equation for determining the corresponding constants A^a and B^a, and the transcendental equation

$$\Phi - \frac{1}{\Psi} = 0\,, \tag{54}$$

where Φ and Ψ are the functions defined by (52)–(53). This equation can be used for determining the eigenvalues corresponding to antisymmetric EFs. These representations and equations differ from (48)–(50) in the replacement

$$\cosh \to \sinh \quad \text{and} \quad \sinh \to \cosh \ . \tag{55}$$

5. Properties of the transcendental and algebraic parts

In the following, we will investigate the properties of the functions Φ and Ψ, when λ is in the range $0 \leq \lambda \leq 1$. Unlike in the isotropic case, the decoupling between the geometric and material parameters is very minimal. The function Ψ does not depend on μ (geometry), but both Φ and Ψ depend on all of the independent material parameters (ν_{12}, E_1, E_2 and G_{12}).

We start our examination by noting that (by direct calculation)

$$\Phi(\lambda_{\min}) = 1 \tag{56}$$

$$\Psi(\lambda_{\min}) = 1 \tag{57}$$

and

$$\Phi(1) = 0 \tag{58}$$

regardless of the problem parameters. We defer the evaluation of the limit $\Psi(\lambda \to \lambda_{\max})$ to the subsection on the algebraic part below, because, although it is trivial to see that Ψ has a singularity there (because $\kappa_- \to 0^+$ as $\lambda \to \lambda_{\max}$), to deduce its sign we need to know the sign of each of the terms in (53).

Let us fix the values of ν_{12}, E_1, E_2 and G_{12} to those corresponding to some given orthotropic material. The qualitative behavior of the functions Φ and Ψ is illustrated in Figure 2. The range for γ (defined by (35)) is obtained by taking the square root of (45). Note that the x axis of the figure starts at $\gamma_{\min}$. In the isotropic case in our earlier study, we had $\gamma_{\min} = 0$, which does not hold for the general orthotropic case.

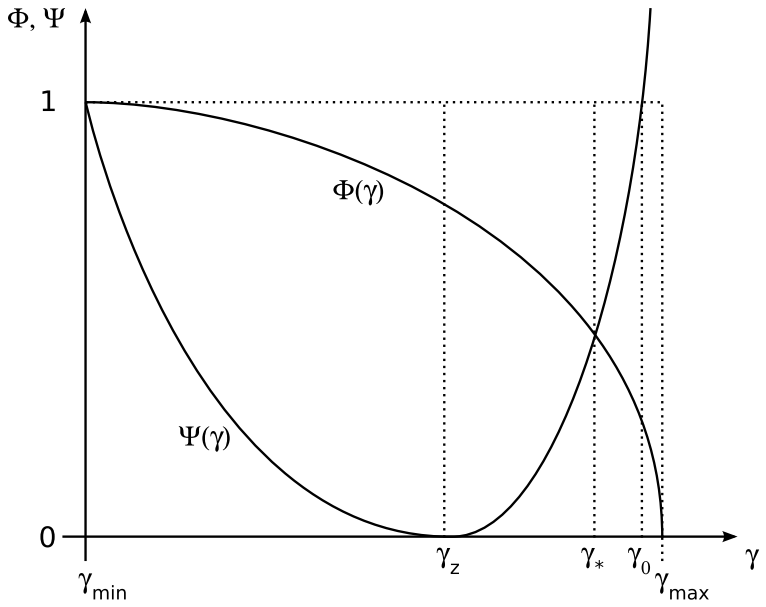

Figure 2: Behaviour of Φ and Ψ as a function of γ when the parameters D_1, D_2, D_3, μ, β_1 and β_2 are fixed. Qualitative drawing.

Figure 3 shows some examples of Φ and Ψ plotted for some general orthotropic materials. Note that as was discussed above, only Φ depends on the aspect ratio $\ell/2b$. We see that the case $G_{12} = G_H$ behaves like the isotropic case, as expected (compare Banichuk et al. 2010). When the value of G_{12} deviates from the Huber estimate, it is seen that when $G_{12} < G_H$, the curvature of Φ becomes more pronounced, especially for a large aspect ratio (i.e., a long, narrow strip). If $G_{12} > G_H$, the value of both functions at $\gamma = \max(0, \gamma_{\min})$ decreases, again especially for a large aspect ratio in the case of Φ.

As γ increases from $\gamma_{\min}$ to $\gamma_{\max}$, the function $\Phi(\gamma, \mu)$ decreases continuously and monotonically from 1 to 0, i.e.

$$1 \geq \Phi(\gamma, \mu) \geq 0, \quad \frac{\partial \Phi(\gamma, \mu)}{\partial \gamma} < 0, \quad \gamma_{\min} \leq \gamma \leq \gamma_{\max} \tag{59}$$

$$\Phi(\gamma_{\min}, \mu) = \left(\tanh \frac{\kappa -}{\mu} \coth \frac{\kappa_+}{\mu} \right)_{\gamma = \gamma_{\min}} = 1$$

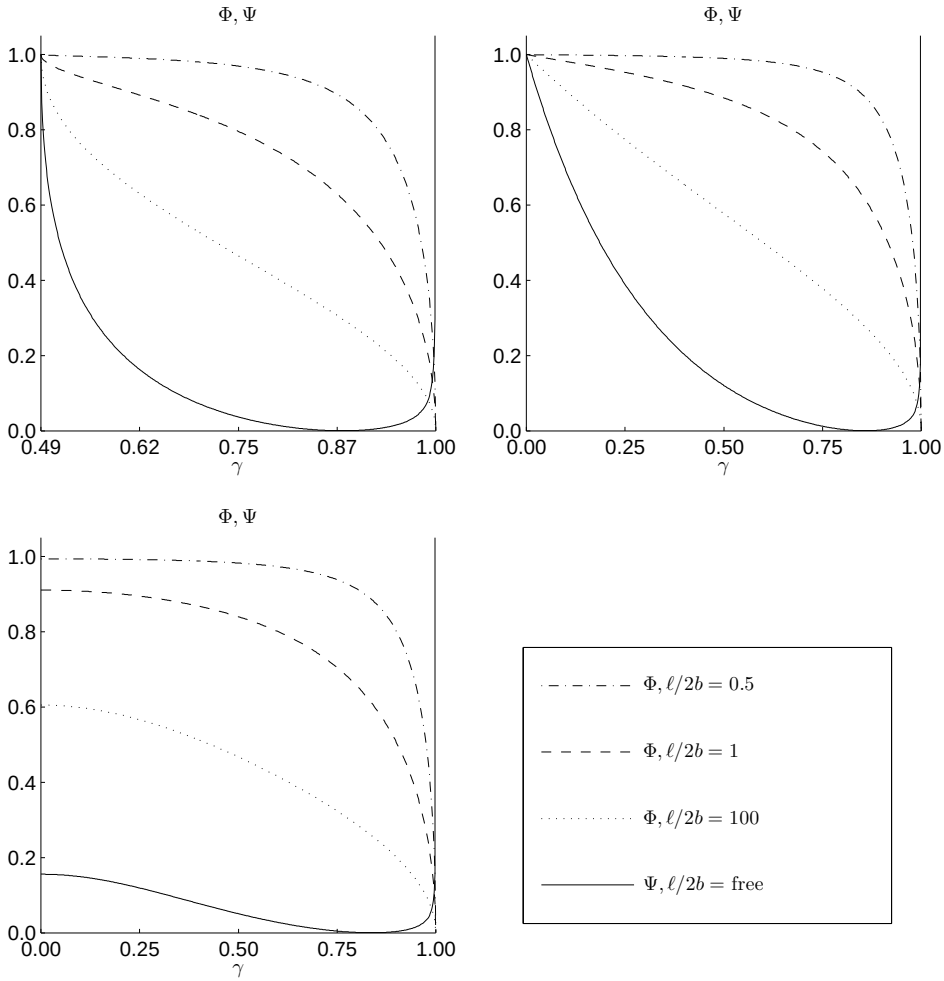

Figure 3: Behaviour of Φ and Ψ for some orthotropic materials, at different aspect ratios $\ell/2b$ and different values for the in-plane shear modulus G_{12}. For all cases, the other material parameters are $E_1 = 6.8$ GPa, $E_2 = 3.4$ GPa and $\nu_{12} = 0.2, \nu_{21} = 0.1$. Note that only Φ depends on the aspect ratio. Upper left: $G_{12} = 0.85\ G_H$ (note the scale for γ). Upper right: $G_{12} = G_H$. Lower left: $G_{12} = 1.15\ G_H$, where G_H is the value given by the Huber estimate (9). The range of γ is $\max(0, \gamma_{\min}) \leq \gamma \leq \gamma_{\max}$, based on (35), (41) and (45), and evaluated separately for each subfigure.

$$\Phi(\gamma_{\max}, \mu) = \left(\tanh \frac{\kappa_-}{\mu} \coth \frac{\kappa_+}{\mu} \right)_{\gamma=\gamma_{\max}} = 0$$

The function $\Psi(\gamma)$ decreases monotonically from 1 to 0 in the interval $\gamma_{\min} < \gamma < \gamma_z$,

$$1 \geq \Psi(\gamma) \geq 0, \quad \frac{\partial \Psi(\gamma)}{\partial \gamma} < 0, \quad \gamma_{\min} < \gamma < \gamma_z \tag{60}$$
$$\Psi(\gamma_{\min}) = 1$$
$$\Psi(\gamma_z) = 0 \,,$$

whereas it increases monotonically in the interval $\gamma_z < \gamma < \gamma_{\max}$ and takes values as large as are desired when $\gamma \to \gamma_{\max}$,

$$0 \leq \Psi(\gamma) < \infty, \quad \frac{\partial \Psi(\gamma)}{\partial \gamma} > 0, \quad \gamma_z < \gamma < 1 \tag{61}$$
$$\Psi(\gamma_z) = 0, \quad \lim_{\gamma \to \gamma_{\max}} \Psi(\gamma) = \infty \,.$$

The function touches zero at the point

$$\gamma_z = \sqrt{\beta_j^2 H_2 - 2\beta_j H_3 + H_1} \,, \tag{62}$$

where $j = 1, 2$. It will be shown below that γ_z is unique. Thus both choices for j obtain the same γ_z.

Because $0 \leq \Phi \leq 1$ for all $\gamma_{\min} \leq \gamma \leq \gamma_{\max}$, the symmetric solution (51) is only possible in the range where $\Psi \leq 1$. Likewise, the antisymmetric solution (54) is only possible in the range where $1/\Psi \leq 1$, i.e., $\Psi \geq 1$. Thus, the value of $\gamma = \gamma_0$ for which $\Psi = 1$, is of special interest. Note that at this point we also have $\Psi = 1/\Psi$ and thus $\Phi - \Psi = \Phi - 1/\Psi$. The functions defined by the left-hand sides of (51) and (54) will therefore cross at the value $\gamma = \gamma_0$.

Note that (60), combined with the consideration in the previous paragraph, implies that the eigenvalue γ_* corresponding to the symmetric solution is always lower than the eigenvalues γ_1 and γ_2 corresponding to the antisymmetric solution. Additionally, since $\Phi(\gamma_{\max}, \mu) = 0$ and $\lim_{\gamma \to \gamma_{\max}} \Psi(\gamma) = \infty$, the second antisymmetric eigenvalue is $\gamma_2 = \gamma_{\max}$. For the various values of γ defined above, we have the ordering $\gamma_{\min} < \gamma_z < \gamma_* < \gamma_0 < \gamma_1 < \gamma_2 = \gamma_{\max}$.

An analytical expression for γ_0 can be found by using the definition (52) – (53) and solving $\Psi^2(\gamma) = 1$ for γ. Let us define the auxiliary expression

$$\alpha \equiv \sqrt{8\,\beta_1\,H_2\,H_3 + \left({\beta_1}^2 - 6\,\beta_1\,\beta_2 + {\beta_2}^2\right)\,{H_2}^2}\,. \tag{63}$$

Then, for the root γ_0 that interests us, the following expression holds:

$$\gamma_0^2 = \frac{1}{2}\left((\beta_2 - \beta_1)\;\alpha + 2\,H_1 - \left({\beta_1}^2 - 4\,\beta_1\,\beta_2 + {\beta_2}^2\right)\;H_2 - 4\,\beta_1\,H_3\right)\,. \tag{64}$$

Using the theory presented, it is possible to numerically find, by first solving γ_* from equation (51), the critical velocity (equation (35)) and the corresponding buckling shape (equations (36), (44), (48) – (50)).

Behaviour of transcendental part: analytical consideration

Let us show that transcendental part Φ is monotonically decreasing in the open interval $(\lambda_{\min}, \lambda_{\max})$. First, we define

$$g(\lambda) \equiv \sqrt{1 - \frac{H_2(H_1 - \lambda)}{H_3^2}}\,, \tag{65}$$

i.e. the square root expression in $\kappa_\pm^2$ in (44). We see that $g(\lambda_{\min}) = 0$ and $g(\lambda_{\max}) = 1$. Between these extreme values, $g(\lambda)$ increases monotonously as λ increases.

We write (44) in the form

$$\kappa_\pm^2 = \frac{1}{H_3}\frac{(1 \pm \sqrt{1 - c(1-\lambda)})}{c}\,, \tag{66}$$

where we have defined the auxiliary constant

$$c \equiv H_2/H_3^2\,.$$

Directly by differentiating (66), we have

$$\frac{\partial(\kappa_\pm^2)}{\partial\lambda} = \frac{\pm 1}{2H_3\sqrt{1 - c(1-\lambda)}}\,, \tag{67}$$

where the upper and lower signs correspond to each other. Note that the square root expression in the denominator is $g(\lambda)$ in (65), and as discussed

above, it takes on values in the range $(0,1)$ as $\lambda \in (\lambda_{\min}, \lambda_{\max})$, and especially is positive in our range of interest. Thus, (67) is always positive for κ_+^2 and always negative for κ_-^2.

On the other hand, by rules of differentiation,

$$\frac{\partial(\kappa_\pm^2)}{\partial\lambda} = 2\kappa_\pm \frac{\partial\kappa_\pm}{\partial\lambda} \,,$$

and thus

$$\frac{\partial\kappa_\pm}{\partial\lambda} = \frac{\partial(\kappa_\pm^2)}{\partial\lambda} / 2\kappa_\pm \,.$$

Noting that $\kappa_\pm > 0$ (in the special case of $\lambda = \lambda_{\max}$, we have $\kappa_- = 0$, but this point is not in our open interval), we have that the signs match:

$$\operatorname{sign} \frac{\partial\kappa_\pm}{\partial\lambda} = \operatorname{sign} \frac{\partial(\kappa_\pm^2)}{\partial\lambda} \,. \tag{68}$$

Now we turn our attention to Φ. Differentiating the definition (52) with respect to λ, we have

$$\begin{aligned}
\frac{\partial\Phi}{\partial\lambda} &= \frac{\partial}{\partial\lambda}\left(\tanh\frac{\kappa_-}{\mu}\right)\coth\frac{\kappa_+}{\mu} + \left(\tanh\frac{\kappa_-}{\mu}\right)\frac{\partial}{\partial\lambda}\left(\coth\frac{\kappa_+}{\mu}\right) \\
&= \frac{1}{\cosh^2\frac{\kappa_-}{\mu}} \cdot \frac{1}{\mu} \cdot \frac{\partial\kappa_-}{\partial\lambda}\coth\frac{\kappa_+}{\mu} + \tanh\frac{\kappa_-}{\mu}\left(-\frac{1}{\sinh^2\frac{\kappa_+}{\mu}}\right)\cdot\frac{1}{\mu}\cdot\frac{\partial\kappa_+}{\partial\lambda} \,.
\end{aligned}$$

In the first term on the right-hand side, $\partial\kappa_-/\partial\lambda < 0$ (by (67) and (68)) while the other factors are all positive, and in the second term, $-1/\sinh^2\frac{\kappa_+}{\mu} < 0$ while all other factors are positive. Thus, both of the terms on the right-hand side are negative and we conclude that

$$\frac{\partial\Phi}{\partial\lambda} < 0 \quad \forall\, \lambda \in (\lambda_{\min}, \lambda_{\max}) \,. \tag{69}$$

Behaviour of algebraic part: analytical consideration

The second part is the algebraic function Ψ. We prove the following results:

1. Ψ has exactly one zero λ_z.
2. Ψ has exactly one singularity, which is located at $\lambda = \lambda_{\max}$, and its sign is positive: $\lim_{\lambda \to \lambda_{\max}} \Psi(\lambda) = +\infty$.
3. If the zero $\lambda_z \in (\lambda_{\min}, \lambda_{\max})$, then Ψ is monotonically decreasing in the interval $\lambda \in (\lambda_{\min}, \lambda_z)$, and monotonically increasing in the interval $\lambda \in (\lambda_z, \lambda_{\max})$.

Again, we begin with (44). We note that the coefficient in front of the expression can be written as

$$\frac{H_3}{H_2} = \frac{D_3}{D_2} = \nu_{12} + 2\frac{G_{12}}{E_2}(1 - \nu_{12}\nu_{21}) .$$

Let us define the constants

$$A \equiv H_3/H_2 = \nu_{12} + 2\frac{G_{12}}{E_2}(1 - \nu_{12}\nu_{21}) , \quad B \equiv 2\frac{G_{12}}{E_2}(1 - \nu_{12}\nu_{21}) . \tag{70}$$

We see that

$$\beta_1 = A - B , \qquad \beta_2 = A + B . \tag{71}$$

Using (70) and (65), definition (44) reduces to a more convenient form,

$$\kappa_{\pm}^2 = A(1 \pm g(\lambda)) . \tag{72}$$

Inserting (71) and (72) into the definition (53), we have

$$\Psi = \frac{\sqrt{A(1+g(\lambda))}(A\,g(\lambda) - B)^2}{\sqrt{A(1-g(\lambda))}(A\,g(\lambda) + B)^2} . \tag{73}$$

All factors in (73) are always positive, except the second one in the numerator. Thus, the function can only have one zero, which is located at such λ_z that $Ag(\lambda_z) - B = 0$. The first result is therefore established.

To prove the second result, we note that there is exactly one singularity, caused by the first term in the denominator as $g(\lambda) \to 1$, i.e. as $\lambda \to \lambda_{\max}$. Ψ is

continuous outside its singularities. Furthermore, from (73) we have that $\Psi \geq 0$ for all λ for which the function is nonsingular. Because Ψ is continuous, the singularity must have the positive sign.

To finish this section, let us show that the third result holds. Note that the special case $A = B$ does not happen as long as $\nu_{12} \neq 0$, which holds for all reasonable materials.

We will now consider the derivative of Ψ with regard to λ. We will for now assume that $\lambda_z \in (\lambda_{\min}, \lambda_{\max})$.

We obtain from (73) that

$$\frac{\partial \Psi}{\partial \lambda} = \frac{\frac{\partial g}{\partial \lambda}\sqrt{A(1-g(\lambda))}(B - A\,g(\lambda))\left(B^2 - A^2 g(\lambda)^2 + 4\,A\,B(g(\lambda)^2 - 1)\right)}{(1-g(\lambda)^2)\sqrt{A(1+g(\lambda))}(A\,g(\lambda)+B)^3} \,. \tag{74}$$

Because all other terms are positive, we have for the sign of the derivative the expression

$$\text{sign}\ \frac{\partial \Psi}{\partial \lambda} = \text{sign}\ \left[(B - A\,g(\lambda))\left(B^2 - A^2 g(\lambda)^2 + 4\,A\,B(g(\lambda)^2 - 1)\right)\right] \,. \tag{75}$$

Note that because $g(\lambda)$ is monotonically increasing (and thus $\partial g/\partial \lambda > 0$), and the zero of Ψ is located at $A\,g(\lambda_z) = B$, we see that

$$\text{sign}\ [A\,g(\lambda) - B] = \text{sign}\ [\lambda - \lambda_z] \,. \tag{76}$$

Thus, the sign of the expression $A\,g(\lambda) - B$ corresponds to whether λ is less or greater than λ_z.

We can write the expression on the right-hand side of (75) as

$$(B - A\,g(\lambda))\left[(B - A\,g(\lambda))\,(B + A\,g(\lambda)) + 4\,A\,B\left(g(\lambda)^2 - 1\right)\right] \,. \tag{77}$$

If $B - A\,g(\lambda) < 0$, i.e. $\lambda > \lambda_z$, the parenthetical expression on the right is negative (note that the last term is always negative because $g(\lambda) < 1$). Thus, in this case we have

$$\frac{\partial \Psi}{\partial \lambda}|_{\lambda > \lambda_z} > 0 \,.$$

The other case $B - A\,g(\lambda) > 0$, i.e. $\lambda < \lambda_z$ is trickier, because then the parenthetical expression on the right hand side of (77) will have one positive and one negative term. The expression represents a parabola with the variable $g(\lambda)$, and has zeroes at

$$g(\lambda) = \pm\sqrt{\frac{4AB - B^2}{4AB - A^2}} \equiv g_0^{\pm} \,. \tag{78}$$

Because $g(\lambda) > 0$, we may discard the negative solution g_0^- in (78). The expression is negative until $g(\lambda)$ becomes larger than the positive solution g_0^+.

The last question that remains is whether this solution lies in our range. We calculate (numerator) $-$ (denominator) from the right-hand side of (78), again look at the definitions (70), and recall that $\nu_{12} > 0$:

$$(4AB - B^2) - (4AB - A^2) = A^2 - B^2 > 0 \,,$$

i.e. the numerator is always larger than the denominator. Thus $g_0^+ > 1$ and the parabola stays negative for our whole range. We have that the total sign is negative and thus

$$\frac{\partial \Psi}{\partial \lambda}|_{\lambda<\lambda_z} < 0 \,.$$

This completes the proof.

6. Numerical solution process

The numerical solution process was similar to the one for the isotropic case in Banichuk et al. (2010), but now the general orthotropic equations were used.

The root $\gamma = \gamma_*$ of equation (51) was searched numerically in the interval $[\gamma_{\min} + \varepsilon_1,\ \gamma_{\max} - \varepsilon_2]$, where the numerical parameters ε_j, $j = 1, 2$, which were used to avoid singularities, were small and determined adaptively based on the sign of $\Phi - \Psi$. The values were initialized as $\varepsilon_j = 10^{-8}$ for both $j = 1, 2$, and each parameter ε_j was halved until the sign of $\Phi - \Psi$ was positive at the left end, and negative at the right end. Then a simple bisection search was

used to locate the root. It was seen that this search for suitable ε_j was necessary especially in the case where $G_{12} < G_H$, because a fixed-size epsilon would skip over the root in some parts of the parameter space (e.g. if E_1/E_2 and ν_{12} were both small).

When $G_{12} < G_H$, it was verified that no roots existed in the tested cases in the interval $\gamma \in [0, \gamma_{\min})$. This was done by minimizing $||f(\lambda)||^2 = f(\lambda) \cdot \overline{f(\lambda)}$, where $f(\lambda) = \Phi(\lambda) - \Psi(\lambda)$, starting from 30 linearly spaced initial guesses in the mentioned interval. Here $\bar{z}$ denotes the complex conjugate of z. Local minima larger than ε were discarded, as were also any duplicates, and any solutions $\gamma \geq \gamma_{\min}$. Note that $\gamma = \gamma_{\min}$ is always a root, corresponding to the trivial solution.

The critical value γ_0 was evaluated from the analytical expression (64), and the root corresponding to the antisymmetric case, $\gamma = \gamma_1$, was found numerically from (54) using $[\gamma_0 + \varepsilon,\ \gamma_{\max} - \varepsilon]$ as the search interval. In this case, the value $\varepsilon = 10^{-8}$ was used.

Once the eigenvalue γ_* of the symmetric case was found, the corresponding eigenfunction was constructed by inserting the eigenvalue into (44), (49) – (50). It is possible to eliminate either A^s or B^s from one of the equations of the system (49) – (50). Either equation can be chosen. Note that the other equation is implicitly used by the zero determinant condition (51).

A numerically stable approach for choosing which constant to eliminate is to test both possibilities, assigning $A^s = 1$ (respectively $B^s = 1$) and calculating B^s (respectively A^s) from the equation system (using, e.g., the first equation). The choice that gives a result that is smaller or equal to 1 is then the one that should be kept. This is necessary, because depending on the problem parameters and this choice, the other constant may be very large, which affects numerical accuracy. (Values up to about 10^{130} were seen.)

We evaluated $w^s(x, y)$ using this choice, and normalised the final result by scaling the maximum value of w^s to unity.

7. Numerical results

When the material parameters E_1, E_2, and ν_{12} are given, the other Poisson ratio ν_{21} can be found from the compatibility condition (17). We see, by numerical tests, that the ratio of the Young moduli E_1 and E_2 is the significant factor affecting the buckling shape, no matter the absolute magnitudes of E_1 and E_2. The value of the in-plane shear modulus G_{12}, as a fraction of the Huber estimate (9), is also seen to affect the buckling shape. See Figure 5.

In addition to the material parameters, we have one geometric parameter, $\ell/2b$, which describes the ratio of the plate's length to its width. The effect of the problem geometry on the displacement localisation phenomenon was investigated in Banichuk et al. (2010). It was observed that when the plate is short and wide ($\ell/2b$ small), the localisation is more pronounced, that is, most of the displacement occurs near the free edges.

The same effect is observed to occur for the orthotropic model, so in order to concentrate on the effect of orthotropy, we will not produce an aspect ratio comparison here. In our following analysis, we will fix $\ell/2b = 0.01$ for the rest of the discussion, as a representative numerical example that exhibits the localisation effect. This is realistic for a short open draw in a paper machine ($\ell = 0.1$ m, $b = 5$ m).

The numerical results are arranged as follows. Figure 4 represents the case of one isotropic material, similar to those presented in Banichuk et al. (2010), and includes some orthotropic variants based on the Huber estimate (9). The subfigure on the left shows the complete buckling shape, while the subfigure on the right displays a slice of the shape at $x = \ell/2$ (corresponding to the bolded line in the left subfigure). It is observed that when the Huber estimate is used, the qualitative behaviour agrees with the isotropic case, as expected. Quantitatively, we see the effect of the Young modulus ratio E_1/E_2. The smaller the ratio is, the more the shape is localised near the free edges.

Figure 5 shows the effect of the in-plane shear modulus G_{12} for general or-

thotropic materials. The left column displays complete buckling shapes, while the right column shows the strength of the localisation effect that was discussed in Banichuk et al. (2010). As discussed above, the problem parameters affecting the localisation effect are the aspect ratio $\ell/2b$, the Young modulus ratio E_1/E_2, the Poisson ratio ν_{12}, and the in-plane shear modulus G_{12}.

Briefly stated, the degree of localisation represents the variation of the displacement in the width (y) direction. When localisation is high (in the relative sense), most of the displacement occurs near the free edges. When localisation approaches zero, so does the y dependence, and the displacement profile approaches a cylindrical one. The degree of localisation is computed from a numerical approximation of the integral $\int_{-b}^{b}[1 - f(y)]\ \mathrm{d}y$, where $f(y)$ is the cross-section. See Banichuk et al. (2010) for some more details.

As can be seen in figure 5, the result qualitatively matches the earlier one from the isotropic case, in that the degree of localisation increases as the Poisson ratios increase (i.e. as incompressibility increases). As a new result, we see that the zone, where the relative strength of localisation rapidly increases, shifts toward the right (i.e. toward larger values of ν_{12}) when the ratio G_{12}/G_H is increased.

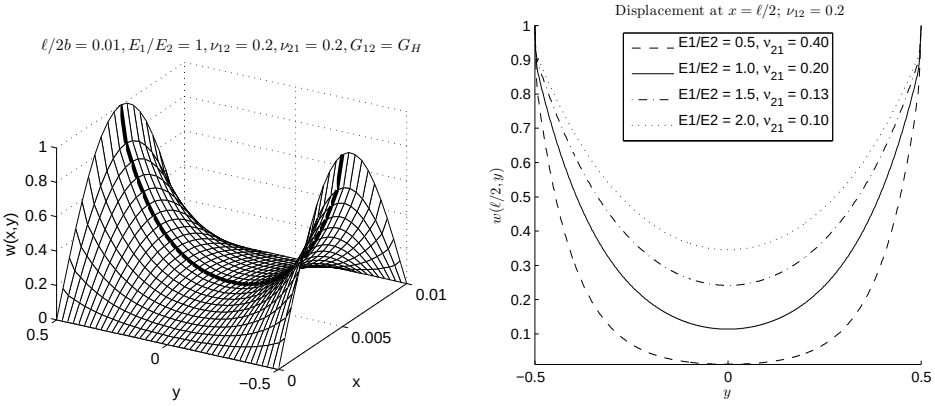

Figure 4: Reference case. Left, symmetric buckling shape for isotropic material, $E = 5$ GPa and $\nu = 0.2$. Aspect ratio $\ell/2b = 0.01$. Right, shape of the profile on the bold line of the left picture. The solid line corresponds to the picture on the left. The dotted lines show the shape of the resulting profile if the isotropic material is replaced with an orthotropic one, while keeping $E_1 = 5$ GPa and $\nu_{12} = 0.2$. The other Poisson ratio ν_{21} is calculated from Maxwell's relation (17), and for G_{12} the Huber estimate (9) is used.

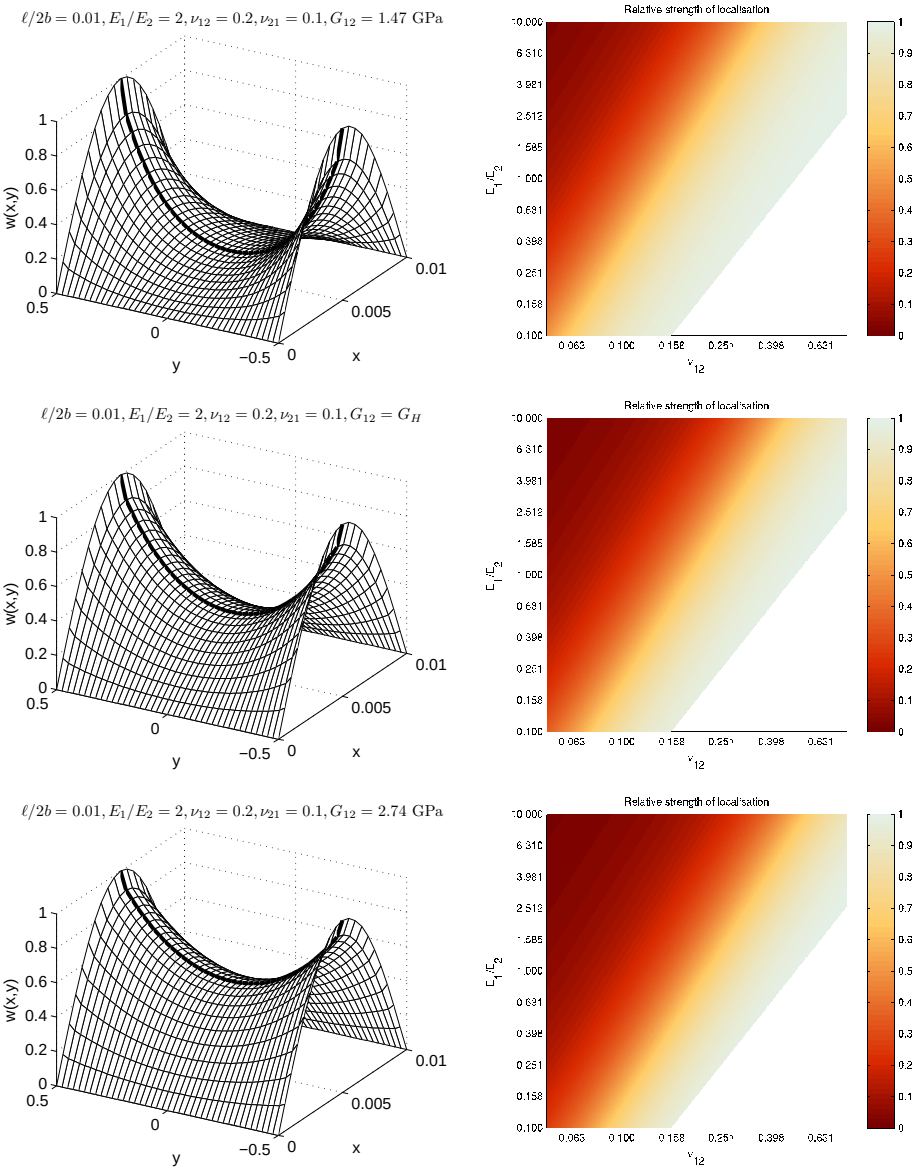

Figure 5: Studied case. Effect of the in-plane shear modulus G_{12}. The aspect ratio is $\ell/2b = 0.01$. The Poisson ratio ν_{21} is calculated from Maxwell's relation (17). Top row: $G_{12} = 0.7\ G_H$, middle row: $G_{12} = G_H$, bottom row: $G_{12} = 1.3\ G_H$, where G_H is the value given by the Huber estimate (9). Left column: symmetric buckling shape for material with $E_1 = 6.8$ GPa, $E_2 = 3.4$ GPa, $\nu_{12} = 0.2$. Right column: relative strength of the localisation effect as a function of Young modulus ratio E_1/E_2 and the Poisson ratio ν_{12}. The effect has been plotted in the area where $\sqrt{\nu_{12}\nu_{21}} \leq 0.5$. The maximum localisation value is normalized to 1 for each subfigure separately, and the reference value G_H is evaluated separately for each point in each plot.

Finally, let us compute the critical divergence velocity for dry paper ($E_1 = 8$ GPa, $E_2 = 0.8$ GPa, $\nu_{12} = 0.8$ ($\nu_{21} = 0.08$)) with an aspect ratio of $\ell/2b = 0.1$, thickness $h = 10^{-4}$ m and mass per unit area $m = 0.08$ kg/m^2, moving in a span of length $\ell = 0.1$ m, and subjected to a tension of $T_0 = 500$ N/m. The estimation (9) is used for the shear modulus G_{12}. By solving equation (35) for V_0 and inserting these values, we obtain $V_0 \approx 79.11$ m/s. We solved two different isotropic limit cases, with $E = E_1 = 8$ GPa and $E = E_2 = 0.8$ GPa. The other parameters were kept the same, and the used Poisson ratio was the geometric average $\nu = \overline{\nu} = \sqrt{\nu_{12}\nu_{21}} = 0.4$. The critical velocities were for the first case $V_0 \approx 79.12$ m/s, and for the second case, $V_0 \approx 79.06$ m/s.

8. Conclusion

In this study, the analytical solution originally developed for isotropic axially moving plates, as reported in Banichuk et al. (2010), was extended to the general orthotropic case. The case was general in the sense that the in-plane shear modulus G_{12} was assumed to be an independent material parameter. The analytical approach allows for a fast solver, which can then be used for applications such as statistical uncertainty and sensitivity analysis, real-time parameter space exploration, and finding optimal values for design parameters.

As a result of applying the developed analytical approach, an explicit expression for the limit velocity of stable axial motion was found, and the limit velocity was computed for an example case. The critical regime was studied as a function of the moduli of orthotropicity. Localised modes of instability of the axially moving orthotropic plate were found in some range of the problem parameters, and the localisation effect was demonstrated with the help of numerical examples.

It was shown analytically that the eigenvalues of the problem determining the shape of the buckled cross-section are nonnegative. The transcendental and algebraic parts of the analytical solution were analyzed in detail, and certain

properties were shown to hold. These properties apply not only to the general orthotropic case, but also to the earlier isotropic one. Thus, the present study also adds details to the analysis in Banichuk et al. (2010).

The buckling shapes were found to depend significantly on the in-plane shear modulus G_{12}. It was observed that if the ratio G_{12}/G_H, where G_H is the geometric average shear modulus, is increased, then the degree of localisation of the deformation to near the free boundaries decreases.

However, for estimation of the critical velocity, the orthotropicity of the material was found to have a negligible effect. Thus, if one aims only to estimate the critical velocity, the isotropic model is sufficiently accurate. The orthotropic and isotropic buckling shapes were confirmed to be qualitatively similar. The main difference was found in the expressions which represent the condition that the boundary conditions are fulfilled.

Finally, some brief observations were made. It was noted that although a prescribed tension value was assumed, the analysis easily generalizes to the case where the x-direction displacement at one of the rollers is prescribed instead. It was also briefly stated that the classical reduction technique, bringing the equations to isotropic form in the case where the geometric average in-plane shear modulus is used, works also for the dynamic case of an axially moving orthotropic plate, despite the Coriolis effect that is present in this setting.

In the particular context of paper production, further expansion of the present model is still needed to account for all of the relevant physical effects. Especially, the interaction between the travelling web and the surrounding air should be taken into account. The effect of the viscoelastic nature of paper on the instability behaviour is another possible topic for further investigation.

References

Archibald, F. R., Emslie, A. G., 1958. The vibration of a string having a uniform motion along its length. ASME Journal of Applied Mechanics 25, 347–348.

Banichuk, N., Jeronen, J., Neittaanmäki, P., Tuovinen, T., 2010. On the instability of an axially moving elastic plate. International Journal of Solids and Structures 47, 91–99, doi:10.1016/j.ijsolstr.2009.09.020.

Biancolini, M. E., Brutti, C., Reccia, L., 2005. Approximate solution for free vibrations of thin orthotropic rectangular plates. Journal of Sound and Vibration 288 (1–2), 321 – 344, dOI: 10.1016/j.jsv.2005.01.005.

Bolotin, V. V., 1963. Nonconservative Problems of the Theory of Elastic Stability. Pergamon Press, New York.

Bonnin, A., Huchon, R., Deschamps, M., 2000. Ultrasonic waves propagation in absorbing thin plates: Application to paper characterization. Ultrasonics 37 (8), 555–563, dOI: 10.1016/S0041-624X(99)00106-7.

Chen, G., Coleman, M. P., Ding, Z., 1998. Some corner effects on the loss of selfadjointness and the non-excitation of vibration for thin plates and shells. The Quarterly Journal of Mechanics and Applied Mathematics 51 (2), 213–240, doi:10.1093/qjmam/51.2.213.

Chonan, S., 1986. Steady state response of an axially moving strip subjected to a stationary lateral load. J. Sound Vib. 107, 155–165.

Frondelius, T., Koivurova, H., Pramila, A., 2006. Interaction of an axially moving band and surrounding fluid by boundary layer theory. Journal of Fluids and Structures 22 (8), 1047–1056.

Gorman, D. J., 1982. Free Vibration Analysis of Rectangular Plates. Elsevier North Holland, Inc.

Göttsching, L., Baumgarten, H. L., 1976. Triaxial deformation of paper under tensile load. In: The Fundamental Properties of Paper Related to Its Uses, Vol. 1. Technical Division of the British Paper and Board Industry Federation, pp. 227–252.

Hatami, S., Azhari, M., Saadatpour, M. M., Memarzadeh, P., 2009. Exact free vibration of webs moving axially at high speed. In: AMATH'09: Proceedings of the 15th american conference on Applied mathematics. World Scientific and Engineering Academy and Society (WSEAS), Stevens Point, Wisconsin, USA, pp. 134–139, houston, USA.

Huber, M. T., 1923. Die theorie des kreuzweise bewehrten eisenbetonplatten. Der Bauingenieur 4, 354–392.

Kikuchi, N., 1986. Finite Element Methods in Mechanics. Cambridge University Press, Cambridge, UK.

Kshirsagar, S., Bhaskar, K., 2008. Accurate and elegant free vibration and buckling studies of orthotropic rectangular plates using untruncated infinite series. Journal of Sound and Vibration 314 (3–5), 837 – 850, dOI: 10.1016/j.jsv.2008.01.013.

Kulachenko, A., Gradin, P., Koivurova, H., 2007. Modelling the dynamical behaviour of a paper web. part ii. Computers & Structures 85, 148–157.

Lin, C. C., 1997. Stability and vibration characteristics of axially moving plates. Int. J. Solids Structures 34 (24), 3179–3190.

Lin, C. C., Mote, C. D., 1995. Equilibrium displacement and stress distribution in a two-dimensional, axially moving web under transverse loading. ASME Journal of Applied Mechanics 62, 772–779.

Lin, C. C., Mote, C. D., 1996. Eigenvalue solutions predicting the wrinkling of rectangular webs under non-linearly distributed edge loading. Journal of Sound and Vibration 197 (2), 179–189.

Mann, R. W., Baum, G. A., Habeger, C. C., 1980. Determination of all nine orthotropic elastic constants for machine-made paper. Tappi Journal 63 (2), 163–166.

Miranker, W. L., 1960. The wave equation in a medium in motion. IBM J. R&D 4, 36–42.

Mote, C. D., 1968. Divergence buckling of an edge-loaded axially moving band. Int. J. Mech. Sci. 10, 281–195.

Mote, C. D., 1972. Dynamic stability of axially moving materials. Shock Vib. Dig. 4 (4), 2–11.

Mote, C. D., 1975. Stability of systems transporting accelerating axially moving materials. ASME Journal of Dynamic Systems, Measurement, and Control, 96–98.

Pramila, A., 1986. Sheet flutter and the interaction between sheet and air. TAPPI-Journal 69 (7), 70–74.

Sagan, H., 1961. Boundary and Eigenvalue Problems in Mathematical Physics. John Wiley & Sons, Inc., slightly corrected reprint by Dover Publications, Inc., 1989.

Seo, Y. B., 1999. Determination of in-plane shear properties by an off-axis tension method and laser speckle photography. Journal of Pulp and Paper Sciences 25 (9), 321–325.

Shin, C., Chung, J., Kim, W., Sep 2005. Dynamic characteristics of the out-of-plane vibration for an axially moving membrane. Journal of Sound and Vibration 286 (4-5), 1019–1031.

Simpson, A., 1973. Transverse modes and frequencies of beams translating between fixed end supports. J. Mech. Eng. Sci. 15, 159–164.

Skowronski, J., Robertson, A. A., 1985. A phenomenological study of the tensile deformation properties of paper. Journal of Pulp and Paper Sciences 11 (1), J21–J28.

Swope, R. D., Ames, W. F., 1963. Vibrations of a moving threadline. J. Franklin Inst. 275, 36–55.

Thorpe, J. L., 1981. Paper as an orthotropic thin plate. TAPPI-Journal 64 (3), 119–121.

Timoshenko, S. P., Woinowsky-Krieger, S., 1959. Theory of plates and shells, 2nd Edition. New York : Tokyo : McGraw-Hill.

Ulsoy, A. G., Mote, C. D., 1980. Analysis of bandsaw vibration. Wood Science 13, 1–10.

Ulsoy, A. G., Mote, C. D., 1982. Vibration of wide band saw blades. ASME Journal of Engineering for Industry 104, 71–78.

Weinstock, R., 2008 (reprint). Calculus of Variations — With Applications to Physics and Engineering. Weinstock Press, isbn 978-1443728812.

Wickert, J. A., Mote, C. D., 1990. Classical vibration analysis of axially moving continua. J. Appl. Mech. 57, 738–744.

Xing, Y., Liu, B., 2009. New exact solutions for free vibrations of rectangular thin plates by symplectic dual method. Acta Mech Sinica 25, 265–270.

Yokoyama, T., Nakai, K., 2007. Evaluation of in-plane orthotropic elastic constants of paper and paperboard. In: 2007 SEM Annual Conference & Exposition on Experimental and Applied Mechanics.

Figure captions

Figure 1: Axially moving elastic orthotropic band, simply supported at $x = 0$ and $x = \ell$.

Figure 2: Behaviour of Φ and Ψ as a function of γ when the parameters D_1, D_2, D_3, μ, β_1 and β_2 are fixed. Qualitative drawing.

Figure 3: Behaviour of Φ and Ψ for some orthotropic materials, at different aspect ratios $\ell/2b$ and different values for the in-plane shear modulus G_{12}. For all cases, the other material parameters are $E_1 = 6.8$ GPa, $E_2 = 3.4$ GPa and $\nu_{12} = 0.2, \nu_{21} = 0.1$. Note that only Φ depends on the aspect ratio. Upper left: $G_{12} = 0.85\ G_H$ (note the scale for γ). Upper right: $G_{12} = G_H$. Lower left: $G_{12} = 1.15\ G_H$, where G_H is the value given by the Huber estimate (9). The range of γ is $\max(0, \gamma_{\min}) \leq \gamma \leq \gamma_{\max}$, based on (35), (41) and (45), and evaluated separately for each subfigure.

Figure 4: Reference case. Left, symmetric buckling shape for isotropic material, $E = 5$ GPa and $\nu = 0.2$. Aspect ratio $\ell/2b = 0.01$. Right, shape of the profile on the bold line of the left picture. The solid line corresponds to the picture on the left. The dotted lines show the shape of the resulting profile if the isotropic material is replaced with an orthotropic one, while keeping $E_1 = 5$ GPa and $\nu_{12} = 0.2$. The other Poisson ratio ν_{21} is calculated from Maxwell's relation (17), and for G_{12} the Huber estimate (9) is used.

Figure 5: Studied case. Effect of the in-plane shear modulus G_{12}. The aspect ratio is $\ell/2b = 0.01$. The Poisson ratio ν_{21} is calculated from Maxwell's relation (17). Top row: $G_{12} = 0.7\ G_H$, middle row: $G_{12} = G_H$, bottom row: $G_{12} = 1.3\ G_H$, where G_H is the value given by the Huber estimate (9). Left column: symmetric buckling shape for material with $E_1 = 6.8$ GPa, $E_2 = 3.4$ GPa, $\nu_{12} = 0.2$. Right column: relative strength of the localisation effect as a function of Young modulus ratio E_1/E_2 and the Poisson ratio ν_{12}. The effect has been plotted in the area where $\sqrt{\nu_{12}\nu_{21}} \leq 0.5$. The maximum localisation value is normalized to 1 for each subfigure separately, and the reference value G_H is evaluated separately for each point in each plot.